HHS Public Access

Author manuscript

J Magn Reson Imaging. Author manuscript; available in PMC 2018 February 01.

Published in final edited form as:

J Magn Reson Imaging. 2017 February ; 45(2): 463–471. doi:10.1002/jmri.25394.

"Pulmonary MRI of neonates in the intensive care unit using 3D ultrashort echo time and a small foot-print MRI system"

Andrew D. Hahn, PhD[1], **Nara S. Higano, MS**[2,3], **Laura L. Walkup, PhD**[2], **Robert P. Thomen, MS**[2,3], **Xuefeng Cao, MS**[2,4], **Stephanie L. Merhar, MD, MS**[5], **Jean A. Tkach, PhD**[6], **Jason C. Woods, PhD**[#2,3], and **Sean B. Fain, PhD**[#1]

[1]Department of Medical Physics, University of Wisconsin, Madison, WI

[2]Center for Pulmonary Imaging Research, Division of Pulmonary Medicine and Department of Radiology, Cincinnati Children's Hospital Medical Center, Cincinnati, OH

[3]Department of Physics, Washington University in St. Louis, St. Louis, MO

[4]Department of Physics, University of Cincinnati, Cincinnati, OH

[5]Perinatal Institute, Division of Neonatology, Cincinnati Children's Hospital Medical Center, Cincinnati, OH

[6]Imaging Research Center, Department of Radiology, Cincinnati Children's Hospital Medical Center, Cincinnati, OH

[#] These authors contributed equally to this work.

Abstract

Purpose—To determine feasibility of pulmonary MRI of neonatal lung structures enabled by combining two novel technologies: first, a 3D radial ultrashort echo time (UTE) pulse sequence capable of high spatial resolution full-chest imaging in non-sedated quiet-breathing neonates, and second, a unique, small-footprint 1.5T MRI scanner design adapted for neonatal imaging and installed within the Neonatal Intensive Care Unit (NICU).

Materials and Methods—Ten patients underwent MRI within the NICU, in accordance with an approved Institutional Review Board protocol. Five had clinical diagnoses of bronchopulmonary dysplasia (BPD), and five had putatively normal lung function. Pulmonary imaging was performed at 1.5T using 3D radial UTE and standard 3D fast gradient recalled echo (FGRE). Diagnostic quality, presence of motion artifacts, and apparent severity of lung pathology were evaluated by two radiologists. Quantitative metrics were additionally used to evaluate lung parenchymal signal.

Results—UTE images showed significantly higher signal in lung parenchyma ($p < 0.0001$) and fewer apparent motion artifacts compared to FGRE ($p = 0.046$). Pulmonary pathology was more severe in patients diagnosed with BPD relative to controls ($p = 0.001$). Infants diagnosed with BPD also had significantly higher signal in lung parenchyma, measured using UTE, relative to controls ($p = 0.002$).

Corresponding author: Sean B. Fain, sfain@wisc.edu, phone: 608.263.0090, fax: 608.265.9840, **Institution of Origination:** University of Wisconsin – Madison, Department of Medical Physics, 1111 Highland Ave., Room 1005, Madison, WI 53705-22.

Conclusion—These results demonstrate the technical feasibility of pulmonary MRI in free-breathing, non-sedated infants in the NICU at high, isotropic resolutions approaching that achievable with CT. There is potential for pulmonary MRI to play a role in improving how clinicians understand and manage care of neonatal and pediatric pulmonary diseases.

Keywords

pulmonary MRI; UTE; bronchopulmonary dysplasia; neonates; lung; 3D radial

Introduction

The rate of neonatal pulmonary morbidity is high among neonatal intensive care unit (NICU) patients (1); however, widely available diagnostic imaging tools are insufficient for the assessment of underlying structural pathologies in this population. Chest radiography is the most common imaging tool in the NICU, given its accessibility and effectiveness for diagnosis of acute pulmonary complications, yet its limited sensitivity to pathological progression reduces its utility for longitudinal monitoring of disease (2). Computed tomography (CT) provides exceptional imaging of pulmonary structures including the lung parenchyma and airways and is considered the ‘gold standard’ technique for lung imaging. However, repeated exposure to ionizing radiation carries significant risk to patient safety if used for routine or longitudinal assessment of pediatric lung disease (3,4).

Magnetic resonance imaging (MRI) is a potential imaging choice for neonates since it provides 3D, high-resolution imaging without ionizing radiation. Unfortunately, pulmonary MRI faces challenges for neonatal applications due to the specific anatomy of the lungs and generally limited access of NICU patients to MRI. MRI has traditionally performed poorly in the lungs because of limited parenchymal signal due to the low proton density (5) and short T_2^* (< 2 ms) properties (6,7) associated with the parenchymal microstructure and air-tissue interfaces of the alveoli. Furthermore, MRI is time-inefficient compared to x-ray techniques, making pulmonary MRI vulnerable to respiratory and cardiac motion (the rate of each is elevated in the neonate as compared to adults). Recent advances in ultrashort echo time (UTE) MRI with 3D radial trajectories have shown promise in addressing the challenges of pulmonary imaging in adults (8-11). These studies have demonstrated 3D whole-chest coverage, reduced sensitivity to cardiac motion, and increased signal-to-noise, especially in the parenchymal lung tissues. Although scan times last several minutes, robust respiratory gating has been used to successfully mitigate the effect of respiratory motion on image quality in adults (8,10,12).

The aim of this study was to demonstrate the feasibility of a novel application of MRI in NICU patients. Specifically, our goal was the preliminary evaluation of pulmonary MRI of neonatal lung structures implemented by combining two state of the art technologies which address the aforementioned challenges: first, a 3D radial UTE pulse sequence capable of high spatial resolution full-chest imaging in non-sedated, free-breathing or mechanically-ventilated neonates, and second, a unique, small-footprint 1.5T MRI scanner design adapted for neonatal imaging and installed within the NICU (13).

Materials and Methods

Facilities and Equipment

All imaging described in this work was performed in the NICU at Cincinnati Children's Hospital Medical Center (CCHMC), which contains a unique, small-footprint 1.5T orthopedic scanner (ONI Medical Systems, currently GE Healthcare, Waukesha, WI), modified for neonatal imaging (14). It features a 21.8-cm open bore, which is reduced to either 18 cm or 16 cm in diameter after insertion of either of two quadrature birdcage body coils (the largest of which is able to accommodate infants up to approximately 4.5 kg). The gradient system, while constructed from ONI Medical Systems hardware (70 mT/m and 300 T/m/s for gradient amplitude and slew rate, respectively), is controlled using GE HDx software that restricts the allowable gradient amplitude and slew rate to 33 mT/m and 120 T/m/s, respectively.

Patient Information

A total of 10 CCHMC NICU patients were recruited for MRI, with Institutional Review Board approval and parental informed consent. This cohort consisted of both infants with a clinical diagnosis of bronchopulmonary dysplasia (BPD, N=5) and infants without a clinical indication of respiratory dysfunction (controls, N=5). Diagnoses were made by a neonatologist with 5 years of experience (SM). BPD diagnosis criteria were based on previously published definitions (15). This patient group partially overlaps with subject cohorts from previously published work involving either non-UTE related MRI in neonates (14), retrospective respiratory gating using UTE MRI (16) or abstracts covering preliminary development of the UTE work fully described here (17,18,19). Relevant demographic information is provided for each subject in **Table 1**. Patient ID, which is used throughout the remainder of this document to refer to individual patients, is determined by indicating the patient's group (Control or BPD) followed by a number indicating the chronological order in which scans were acquired within each group (BPD1-5 and Control1-5). Patients are listed in **Table 1** according to the overall chronological order in which scans were acquired.

Prior to MRI, infants were evaluated to confirm that their condition was appropriately stable for scanning, and were then prepared for examination using the "feed and swaddle" method (20). All subjects were imaged without intra-venous contrast agents. No sedation was administered as a part of this study, though Control1 and BPD4 received sedation (Midazolam) as part of a clinically-ordered MRI scan that immediately preceded the research scan. Infants were equipped with standard hearing protection, and respiratory and cardiac function were monitored continuously throughout the exam. Subjects were allowed to breathe freely during scanning with the exception of BPD4, in which case an MR-compatible ventilator provided clinically-indicated respiratory support. Additionally, Patients BPD1 and BPD2 were on nasal cannula at the time of their MRI. Patient BPD4 also underwent a clinically-ordered CT exam.

Image Acquisition

A custom 3D radial, radio frequency (RF) spoiled UTE pulse sequence was implemented on the CCHMC NICU scanner (**Figure 1a**), employing a pulse sequence design adapted from

Johnson et al. (10) to conform to the spatial resolution requirements of neonatal MRI. Specific patient-wise acquisition parameters are provided in **Table 2**. Patients are listed in **Table 2** in overall chronological order of scan acquisition, as in **Table 1**.

A number of minor modifications were made to the pulse sequence originally developed for adults (10) for adaptation to neonatal imaging. The schematic diagram of the neonatal pulse sequence structure is shown in **Figure 1b**. First, the readout duration was extended from 1 ms to 2 ms to improve image resolution by a factor of 2 while maintaining an adequate variable-density readout gradient pulse-shape and its associated benefits to signal-to-noise ratio (SNR). Second, the selectively excited slab width was narrowed to 12 cm due to the smaller size of the neonatal torso relative to adults. This increased the amount of time required to refocus the through slab phase (shaded region in **Figure 1b)**, and thus also increased the minimum achievable echo time (TE) to ~200 μs. Compared to the 80-μs TE reported previously in adults (10), a 200-μs TE results in an 11.3% and 5.8% relative reduction in SNR in tissues with a 1-ms and 2-ms T_2^* relaxation rate, respectively. Finally, view ordering was pseudo-randomized to allow reconstruction from a generally arbitrary subset of all acquired data (**Figure 1c**).

Deviations between the prescribed and actual readout trajectory are generated by variations in the gradient amplitudes and timings and can lead to reduced image quality and artifacts in non-Cartesian trajectories (21). Trajectory errors were measured from separately acquired ~1-min calibration phantom scans that followed each neonatal exam using the method described in Duyn et al (21).

Axial Cartesian 3D fast gradient recalled echo (FGRE) images were also acquired using a product sequence for comparison to the UTE images. Relevant FGRE sequence parameters were: TR/TE ~7/1.9 ms; 10° flip angle; 18-20 cm FOV; 0.70-0.78 mm × 0.70-0.78 mm × 3 mm spatial resolution; 5-10 averages; total scan time ~5-10 min.

Finally, a clinically ordered CT (Toshiba, Aquilon ONE, FC56 reconstruction kernel) was acquired without contrast in a single patient (BPD4) at inspiration with a spatial resolution of 0.39 mm × 0.39 mm × 3 mm.

Image Reconstruction

UTE data acquired during periods of intermittent bulk motion were manually identified and discarded by inspecting the repeatedly sampled center of k-space (i.e. the initial point of the free induction decay) acquired as the first sample in each TR (**Figure 1d**). Iteratively estimated sampling density compensation weights (22) were applied to the data to account for non-uniformly sampled k-space, which was then interpolated onto a regular Cartesian grid (23). Inverse Fourier transform of the re-gridded k-space yielded the final images.

Quantitative Analysis

Two radiologists (≥8 years of experience) evaluated each of the 20 imaging data sets (10 UTE and 10 FGRE, which were anonymized and presented in random order) with respect to diagnostic image quality, apparent severity of lung parenchymal pathology, and severity of apparent motion artifacts. Diagnostic quality, specifically related to regions of the lung, was

assigned a score of 1-5; scores of 1, 3 and 5 corresponded to non-diagnostic, moderate and excellent, respectively. Degree of structural parenchymal pathology was also given a score of 1-5, ranging from none (score of 1) to severe (score of 5). Finally, apparent presence of cardiac motion artifacts were assessed separately from appearance of all other motion related artifacts, including artifacts related to respiratory and/or bulk motion, including blurring. Again, a score of 1-5 was assigned for each, ranging from none (score of 1) to severe (score of 5).

Parenchymal lung tissue signal was quantified by normalizing to muscle tissue signal. This was accomplished by taking the mean signal within 6 different ROIs in the upper, middle and lower region of each lung (each located medially along the anterior-posterior axis) and expressing them as a percentage of the mean signal within the muscle tissue. Lung parenchymal SNR was estimated by dividing the ROI means by the standard deviation of the noise in a large, background ROI. ROI placement and size were consistent between subjects and imaging sequences (i.e. UTE and FGRE). Additionally, effort was made to avoid large vessels and significant regions of obvious pathology (i.e. very intense signal), when possible.

Comparison of quantitative metrics between imaging sequences and between BPD and control groups was made using ANOVA. Comparisons were considered statistically significant for p-values < 0.05.

Results

Results from UTE acquisitions in all 10 subjects are shown in both axial and coronal planes in **Figure 2**. Diagnostic image quality was, on average moderate-to-good (score of 3.65 ± 0.93). In 9 out of 10 cases, diagnostic quality was moderate or better (score ≥3), while 1 case (BPD2, both readers) had poor diagnostic quality (score of 2); none of the UTE images were considered non-diagnostic. Note that for BPD1 the data were reconstructed at half the nominal resolution in all 3 axes (from 0.7 mm to 1.4 mm isotropic resolution) due to a combination of insufficient data sampling and significant bulk motion, (~38,000 projections acquired, ~15,000 accepted for reconstruction). At lower resolution, good parenchymal signal sensitivity is maintained in BPD1's images (63% ± 7.4% of muscle tissue across the 6 ROIs) and moderate-to-good diagnostic quality is achieved (scores of 3 and 4). Each reader scored all but 1 of the UTE images as free of apparent cardiac motion artifacts, and all but 2 (both scores given by reader 1) were free of any bulk or respiratory motion artifacts. On average, scores of apparent motion artifacts were 1.1 ± 0.31 and 1.15 ± 0.49 for cardiac and respiratory/bulk motion, respectively. Quantitatively, parenchymal signal measurements were, on average 53% ± 9.8% of muscle signal, with a range of 38.9% − 81.1% across all 60 ROIs. Lung parenchymal SNR was 5.1 ± 1.01, while muscle SNR was 9.98 ± 2.28.

Radiologist scoring of the severity of parenchymal pathology from UTE images was 2.3 ± 0.48 and 3.7 ± 1.06 for control and BPD patient groups, respectively. This difference was significant, with $p = 0.0013$. BPD patients also showed elevated parenchymal signal (56.9% ± 10.7% of muscle signal, range of 40.0% − 81.1%), relative to controls (49.3% ± 7.2%, range of 38.9% − 62.8%). This difference was significant with $p = 0.002$.

Diagnostic quality of the 3D UTE results (3.65 ± 0.93) was comparable to that obtained using the product 3D FGRE (4.05 ± 1.00). These differences were not significant (p = 0.20). Examples of both UTE and FGRE images are shown for several subjects in **Figure 3**, along with a clinically ordered CT in BPD4. First, the higher, isotropic 3D resolution of the UTE is emphasized in coronal-plane reconstructions in contrast with the 3 mm through-slab resolution of the FGRE acquisition. These data also emphasize the appreciably higher parenchymal signal in UTE images. Parenchymal signal was 53% ± 9.8% (range of 38.9% − 81.1%) with UTE vs. 28.3% ± 10.0% (range of 14.8% − 65.9%) with FGRE, which are significantly different ($p = 3.81\times10^{-26}$). Additionally, the absence of artifacts from respiratory and bulk motion is evident in the UTE compared to FGRE images, where minor motion artifacts are visible in the latter (Figure 2, arrows). Radiologist scores of cardiac motion artifacts in FGRE were very low, and effectively equivalent to those in UTE (1.1 ± 0.31 for UTE, 1.2 ± 0.37 for FGRE, p = 0.64). Scores for respiratory/bulk motion artifacts, however, were on average more than 50% higher in FGRE than in UTE (1.15 ± 0.49 for UTE, 1.8 ± 1.32 for FGRE), with a significant difference between the two (p = 0.046). Notably, 60% of the FGRE images had scores >1, and 40% had scores of 4 or 5 (significant to severe artifacts) from at least one reader.

Spearman correlation between the scores from each radiologist was 0.76, and the scores themselves are plotted in **Figure 4**. This plot demonstrates that while scores for image quality and lung pathology have generally good agreement (90% differ by ≤1 point), this is not the case for scores of motion artifacts. Scores of motion artifacts only match in cases where both radiologists gave scores of 1. **Table 3** provides the mean and standard deviation of the scores for each of the 4 evaluated categories from each radiologist independently, and with all scores combined. Bulk motion was the only category where mean scores were significantly different between the two radiologists (p = 0.021).

Discussion

Our results demonstrate the feasibility of pulmonary UTE MRI in free-breathing, non-sedated infants in the NICU at high, isotropic resolutions approaching that achievable with CT. 3D radial UTE MR images of diagnostic quality were acquired successfully in all 10 NICU patients evaluated in this study. Regions of parenchymal signal inhomogeneity indicative of structural pathology were generally clearly visible. The ability to visualize fine structures is demonstrated, although more so in certain patients. Understanding the source of inconsistencies in this area is an important focus of ongoing work.

In general terms, the patients without indication of pulmonary dysfunction have relatively homogeneous parenchymal signal throughout the lung. However, Control1 is a notable exception with numerous regions of parenchymal signal increases, likely indicative of sub-clinical structural abnormalities or atelectasis. Patients diagnosed with BPD generally show regional increases (opacities) and decreases (lucencies) in parenchymal signal, likely indicative of fibrosis and/or atelectasis and alveolar simplification, respectively.

Another important finding is that the parenchymal signal as a percentage of muscle tissue in UTE images are comparable to relative attenuation between muscle and lung parenchyma in similarly aged subjects as measured by CT (~50%) (24,25).

Images acquired with UTE demonstrated increased parenchymal signal and fewer artifacts associated with bulk and respiratory motion relative to standard FGRE images, the latter of which are readily obtainable on clinical MRI systems and have been utilized previously to quantify lung disease in neonatal research studies (14). Insensitivity to motion can be attributed to both the 3D radial trajectory (9) as well as retrospective detection of bulk motion using the center of k-space. The flexibility to retrospectively trade scan time for spatial resolution (as in BPD1) highlights another potential advantage of 3D radial UTE in the event that a large majority of data is corrupted by bulk motion in a fidgety subject or if a scan must be terminated early due to patient discomfort.

Major work remains to further improve and characterize the methodology. The gradient waveform calibration discussed above, initially performed on an external phantom, is being integrated into the patient scan itself to improve the ease of use and reliability. Determining optimal acquisition parameters is crucial, particularly related to image resolution and the amount of data that must be acquired to reliably meet a clinically appropriate and consistent standard of image quality. Measurement of parenchymal T_1 and T_2^* in neonates is warranted to determine optimal flip angle, repetition time, and readout durations. For example, the T_1-weighting in the images in the first 9 patients is clear from by the bright fat signal and is the result of using a relatively high flip angle (8°-10°) up until the 10^{th} exam (BPD5), where flip angle was reduced to 5°. This value is closer to the Ernst angle of 5.5°, given our TR ≈ 5 ms and assuming T_1 is similar to that in adult lung parenchyma, ~1.1 sec (26). The improvement in contrast and lung parenchymal SNR for BPD5 is some validation of this assumption, although direct measurement of T_1 in neonatal lung tissue is needed. Regional mapping of T_1 and T_2^* may also have clinical utility as biomarkers of developmental and disease progression.

Improved motion compensation is also an area of active development, especially to make the sequence robust to the many short intermittent bursts of bulk motion occurring in the non-sedated infant. With motion navigators derived from the radial trajectory, it is potentially feasible to retrospectively reconstruct images not only to reduce bulk motion, but at multiple lung inflation volumes throughout the respiratory cycle (16,18,19). This could allow quantification of tidal lung volumes and regional changes in parenchymal density as a function of lung volume, potentially providing local compliance measures relative to ventilation (27,28).

Overall, our goal is to reduce the risks of longitudinal assessment of neonatal pulmonary disease via non-ionizing pulmonary MRI methods that are motion-insensitive and do not require sedation. As more hospitals install MRI scanners sited within their NICUs, the translational feasibility of neonatal MRI will increase. The proposed MRI technologies represent one solution that could improve access to routine use of MRI technology for the diagnosis and study of neonatal lung disease in NICU patients. Ultimately MRI may have an

important influence on the clinical treatment of pulmonary diseases, such as BPD, in this high-risk population.

This study has number of notable limitations. First, the UTE imaging parameters varied widely across subjects during early parameter optimization, which may confound results. Second, in contrast with CT, MRI signal in lung vs. muscle is influenced not only by the water/proton density but by the relative differences in T_1 and T_2^* relaxations. However, relative T_1 weighting in neonatal lung and muscle are likely not significantly different, since these have been reported to both be ~1.1 sec in adults (26,29). In addition, T_2^* weighting is minimal with UTE, so the lung-to-muscle signal ratio is a good approximation of the lung-to-muscle proton density ratio. These assumptions are supported by the good agreement between these measures in UTE vs. similarly reported values from CT (24,25). Third, the SNR in lung parenchyma was quite low (~5 on average), primarily as a consequence of the very high UTE spatial resolution. It is possible the low SNR was a significant factor in the radiologist evaluation of diagnostic quality. Finally, the number of subjects (N=10) also limits the strength of the conclusions to be drawn. Furthermore, all control subjects were NICU patients. Ideally, the pulmonary MRI data collected in the BPD group would be compared to that acquired in an age-matched, non-NICU control cohort.

In conclusion, we have presented results that demonstrate the feasibility of structural pulmonary UTE MRI in NICU patients, with high 3D isotropic spatial resolution. The data acquisition was facilitated by unique and state-of-the-art MRI facilities within the CCHMC NICU, which allow MRI assessment of fragile NICU patients with minimal risk. These initial results demonstrate potential for pulmonary UTE MRI to inform how clinicians understand and manage care of neonatal and pediatric pulmonary diseases.

Acknowledgments

Funding Support: NIH T32 HL007752; The Perinatal Institute at CCHMC; T32 CA009206; The Hartwell Foundation, NIH/NHLBI P01 HL070831

Glossary

BPD	bronchopulmonary dysplasia
CCHMC	Cincinnati Children’s Hospital Medical Center
CT	computed tomography
FGRE	fast gradient recalled echo
GA	gestational age
GI	gastrointestinal
MRI	magnetic resonance imaging
NICU	Neonatal Intensive Care Unit
PMA	post-menstrual age

RF	radio frequency
SNR	signal-to-noise ratio
T	Tesla
TE	echo time
TR	repetition time
wks	weeks
UTE	ultrashort echo time

References

1. Gage S, Kan P, Oehlert J, Gould JB, Stevenson DK, Shaw GM, O'Brodovich HM. Determinants of chronic lung disease severity in the first year of life; A population based study. Pediatric Pulmonology. 2015; 50:878–888. [PubMed: 25651820]
2. Oppenheim C, Mamou-Mani T, Sayegh N, de Blic J, Scheinmann P, Lallemand D. Bronchopulmonary dysplasia: value of CT in identifying pulmonary sequelae. Am J Roentgenol. 1994; 163(1):169–172. [PubMed: 8010206]
3. Brenner DJ, Elliston CD, Hall EJ, Berdon WE. Estimated risks of radiation-induced fatal cancer from pediatric CT. Am J Roentgenol. 2001; 176:289–296. [PubMed: 11159059]
4. Pearce MS, Salotti JA, Little MP, McHugh K, Lee C, Kim KP, Howe NL, Ronckers CM, Rajaraman P, Craft AW, Parker L, de Gonzalez AB. Radiation exposure from CT scans in childhood and subsequent risk of leukaemia and brain tumours: a retrospective cohort study. Lancet. 2012; 380:499–505. [PubMed: 22681860]
5. Coxson HO, Rogers RM, Whittall KP, D'Yachkova Y, Pare PD, Sciurba FC, Hogg JC. A quantification of the lung surface area in emphysema using computed tomography. American journal of respiratory and critical care medicine. 1999; 159:851–856. [PubMed: 10051262]
6. Hatabu H, Alsop DC, Listerud J, Bonnet M, Gefter WB. T2* and proton density measurement of normal human lung parenchyma using submillisecond echo time gradient echo magnetic resonance imaging. Eur J Radiol. 1999; 29:245–252. [PubMed: 10399610]
7. Stock KW, Chen Q, Hatabu H, Edelman RR. Magnetic resonance T-2* measurements of the normal human lung in vivo with ultra-short echo times. Magn Reson Imaging. 1999; 17:997–1000. [PubMed: 10463650]
8. Gibiino F, Sacolick L, Menini A, Landini L, Wiesinger F. Free-breathing, zero-TE MR lung imaging. Magnetic Resonance Materials in Physics, Biology and Medicine. 2014; 28(3):207–215.
9. Weick S, Breuer FA, Ehses P, Hintze C, Biederer J, Jakob PM. DC-gated high resolution three-dimensional lung imaging during free-breathing. J Magn Reson Imaging. 2013; 37(3):727–732. VP, V M. [PubMed: 22987283]
10. Johnson KM, Fain SB, Schiebler ML, Nagle S. Optimized 3D ultrashort echo time pulmonary MRI. Magn Reson Med. 2013; 70(5):1241–1250. [PubMed: 23213020]
11. Dournes G, Grodzki D, Macey J, Girodet PO, Fayon M, Chateil JF, Montaudon M, Berger P, Laurent F. Quiet submillimeter MR imaging of the lung is feasible with a PETRA sequence at 1.5T. Radiology. 2015; 276(1):258–265. [PubMed: 25768672]
12. Schrauben EM, Anderson AG, Johnson KM, Wieben O. Respiratory-induced venous blood flow effects using flexible retrospective double-gating. J Magn Reson Imaging. 2015; 42(1):211–216. [PubMed: 25210850]
13. Tkach JA, Hillman NH, Jobe AH, Loew W, Pratt RG, Daniels BR, Kallapur SG, Kline-Fath BM, Merhar SL, Giaquinto RO, Winter PM, Li Y, Ikegami M, Whitsett JA, Dumoulin CL. An MRI system for imaging neonates in the NICU: initial feasibility study. Pediatr Radiol. 2012; 42(11): 1347–56. [PubMed: 22735927]

14. Walkup LL, Tkach JA, Higano NS, Thomen RP, Fain SB, Merhar SL, Fleck RJ, Amin RS, Woods JC. Quantitative Magnetic Resonance Imaging of Bronchopulmonary Dysplasia in the NICU Environment. Am J Respir Crit Care Med. 2015; 192(10):1215–1222. [PubMed: 26186608]
15. Ehrenkranz RA, Walsh MC, Vohr BR, Jobe AH, Wright LL, Fanaroff AA, Wrage LA, Poole K. Validation of the National Institutes of Health consensus definition of bronchopulmonary dysplasia. Pediatrics. 2005; 116(6):1353–1360. [PubMed: 16322158]
16. Higano NS, Hahn AD, Tkach JA, Cao X, Walkup LL, Thomen RP, Merhar SL, Kingma PS, Fain SB, Woods JC. Retrospective respiratory self-gating and removal of bulk motion in pulmonary UTE MRI of neonates and adults. Magn Reson Med. 2016 doi: 10.1002/mrm.26212.
17. Hahn, AD.; Higano, NS.; Walkup, LL.; Cao, X.; Thomen, RP.; Tkach, JA.; Dumoulin, CL.; Johnson, KM.; Nagle, SK.; Woods, JC.; Fain, SB. Pulmonary MRI of infants in the neonatal intensive care unit: initial experience with 3D radial UTE; Proceedings of the 23rd International Society for Magnetic Resonance in Medicine; Toronto. 2015. p. 1453
18. Hahn, AD.; Cao, X.; Higano, NS.; Tkach, JA.; Walkup, LL.; Thomen, RP.; Nagle, SK.; Lee, G.; Johnson, KM.; Fain, SB.; Woods, JC. Self-gating of respiratory motion for pulmonary ultra short echo time MRI of infants in the NICU; Proceedings of the 23rd International Society for Magnetic Resonance in Medicine; Toronto. 2015. p. 1460
19. Higano, NS.; Hahn, AD.; Walkup, LL.; Thomen, RP.; Merhar, SL.; Cao, X.; Tkach, JA.; Fain, SB.; Woods, JC. Neonatal Lung Imaging during Quiet-breathing via Ultra-short Echo Time (UTE) Proton MRI and Retrospective Respiratory Gating; American Thoracic Society International Conference; Denver. 2015. p. 197
20. Mathur AM, Neil JJ, McKinstry RC, Inder TE. Transport, monitoring, and successful brain MR imaging in unsedated neonates. Pediatr Radiol. 2008; 38:260–264. [PubMed: 18175110]
21. Duyn JH, Yang Y, Frank JA, van der Veen JW. Simple Correction Method fork-Space Trajectory Deviations in MRI. J Magn Reson Imaging. 1998; 132(1):150–153.
22. Pipe JG, Menon P. Sampling density compensation in MRI: rationale and an iterative numerical solution. Magn Reson Med. 1999; 41(1):179–186. [PubMed: 10025627]
23. Jackson J, Meyer CH, Nishimura DG, Macovski A. Selection of a Convolution Function for Fourier Inversion Using Gridding. EEE Trans Med Imaging. 1991; 10(1):473–478.
24. Stein, J.; Walkup, LL.; Fleck, RA.; Woods, JC. CT characterization of normal pediatric lung parenchymal density; Proc of the Society for Pediatric Radiology; Bellevue, Washington, U.S.A.. 2015.
25. Long FR, Williams RS, Castile RG. Inspiratory and expiratory CT lung density in infants and young children. Pediatr Radiol. 2005; 35:677–683. [PubMed: 15821935]
26. Kruger SJ, Fain SB, Johnson KM, Cadman RV, Nagle SK. Oxygen-enhanced 3D radial ultrashort echo time magnetic resonance imaging in the healthy human lung. NMR In Biomedicine. 2014; 27:1535–1541. [PubMed: 24984695]
27. Pennati F, Salito C, Baroni G, Woods JC, Aliverti A. Comparison between multivolume CT-based surrogates of regional ventilation in healthy subjects. Acad Rad. 2014; 21:1268–1275.
28. Pennati F, Quirk JD, Yablonskiy DA, Castro M, Aliverti A, Woods JC. Assessment of regional lung function by multi-volume 1H-MRI in health and obstructive lung disease: comparison with ^{3}He-MRI. Radiology. 2014; 273:580–590. [PubMed: 24937692]
29. Gold GE, Han E, Stainsby J, Wright G, Brittain J, Beaulieu C. Musculoskeletal MRI at 3.0T: relaxation times and image contrast. Am J Roentgenol. 2004; 183(2):343–351. [PubMed: 15269023]

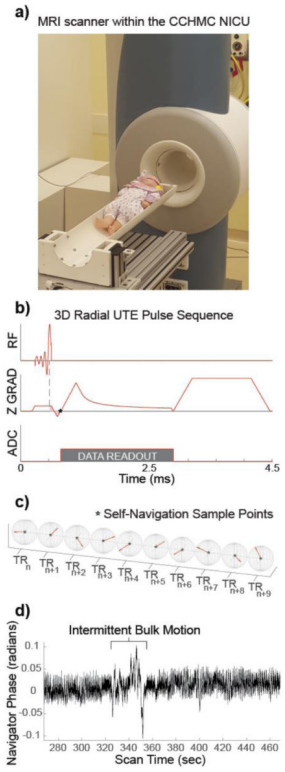

Figure 1.

(a) The MRI scanner located within the CCHMC NICU, with a baby doll placed on the patient table, for reference. (b) The pulse sequence diagram for the UTE sequence. The dotted line indicates the nutation point of the RF pulse, and the area of the pink shaded region is equal to zero at TE, represented by the star (at k-space center) (c) Ten consecutive center-out radial k-space trajectories are shown, highlighting the pseudo-random view ordering and the repeated sampling of the k-space center, indicated again by a star. (d) A 200-sec segment of the phase sampled from the center of k-space during an infant exam, with an example of bulk motion highlighted.

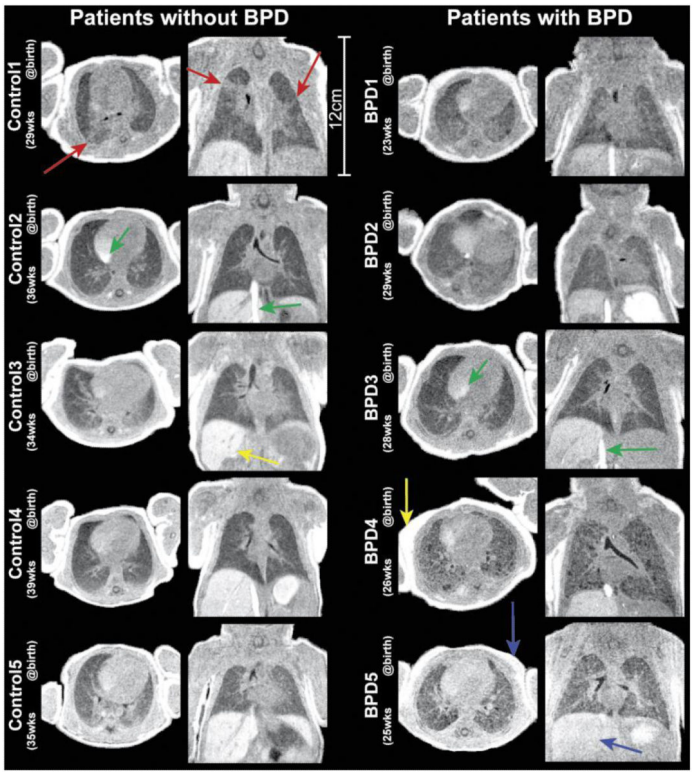

Figure 2.

Views in the axial and coronal planes from 3D UTE image volumes. Patients with no clinical diagnoses of pulmonary disease (left column) are shown alongside patients diagnosed with BPD (right column). Red arrows highlight regions of distinctly heterogeneous parenchymal signal for Control1, a possible indication of sub-clinical pathology potentially linked to the prematurity of birth. Yellow arrows in Control3 and BPD4 highlight the bright liver and fat signal, respectively, associated with heavy T_1 weighting obtained with the use of higher flip angles (8°-10°). Blue arrows show reduced contrast between muscle and both fat and liver in BPD5, predicable from the lower flip angle used (5° vs. 8°-10°). Green arrows highlight inflow effects in the right atrium and inferior vena cava.

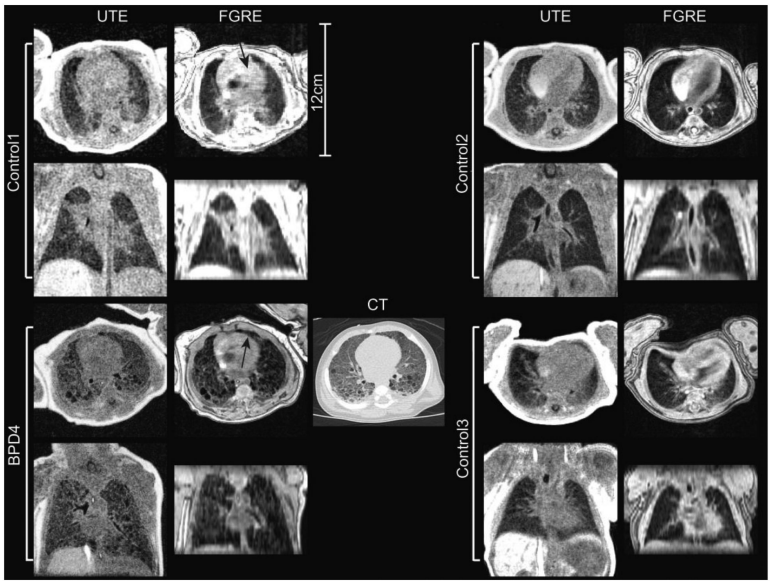

Figure 3.

3D radial UTE and 3D Cartesian FGRE images in 4 different patients. The UTE shows considerably improved sensitivity to parenchymal signal, and structure apparent in FGRE data appears reliably in the UTE as well. The high isotropic resolution of the UTE images is contrasted with the 3-mm S-I resolution of the FGRE data in coronal plane reformats. Regions affected by minor apparent motion artifacts are highlighted by arrows (Control1, axial FGRE; BPD4 axial FGRE). Comparison with clinical CT (performed as part of the NICU standard of care) is also shown for BPD4 (bottom left).

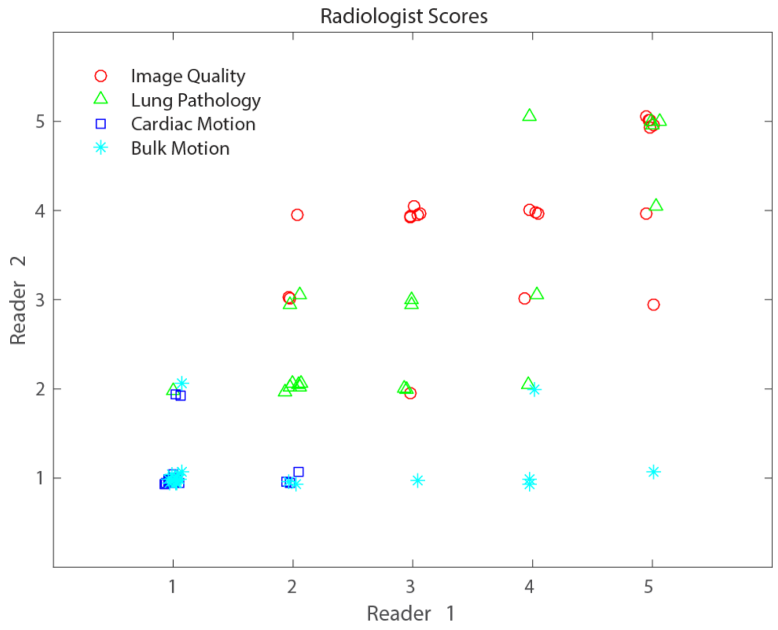

Figure 4.

Scatterplot of scores from each of the 2 radiologists. Points are dithered around whole numbered values for easier visualization. Evaluations of image quality, degree of lung pathology, cardiac motion and bulk motion are shown in red, green, blue and cyan, respectively. Overall, scores are generally well correlated (Spearman correlation = 0.76).

Table 1

NICU Patient Demographic Info

Patient ID	Gender	Gestational age @ birth (wks)	Post-menstrual age @ MRI (wks)	Mass @ Scan (kg)	Condition
BPD1	M	23	38	3.0	BPD (moderate)
Control1	M	29	36	2.7	Control (obstructive hydrocephalus, respiratory distress syndrome, feeding problems)
BPD2	F	29	37	2.3	BPD (moderate)
Control2	F	36	40	3.2	Control (congenital gastroschisis)
BPD3	M	28	40	3.7	BPD (moderate)
BPD4	M	26	39	3.5	BPD (severe, ventilated)
Control3	F	34	38	2.5	Control (apnea, seizures, abnormal heart rhythm, small-for-gestational-age)
Control4	F	39	41	2.6	Control (Hirschsprung's disease)
Control5	F	35	38	2.5	Control (gastroschisis)
BPD5	M	25	43	3.1	BPD (moderate)

Table 2

UTE Acquisition Parameters

Patient ID	# of Radial Projections	Scan Time* (min:sec)	FOV (mm)	Matrix Size	Slab Size (mm)	TE (ms)	TR (ms)	Flip Angle (°)
BPD1	37,976	3:08	180	256	180	0.16	4.9	8
Control1	75,825	5:36	220	256	120	0.16	4.4	10
BPD2	107,967	8:11	220	256	120	0.28	4.5	10
Control2	120,000	10:24	220	256	140	0.25	5.2	10
BPD3	107,899	9:36	220	320	120	0.28	5.3	10
BPD4	119,890	10:29	180	256	120	0.28	5.2	10
Control3	299,982	24:18	180	256	120	0.21	4.9	10
Control4	199,920	16:19	180	256	120	0.21	4.9	10
Control5	199,920	16:19	180	256	120	0.21	4.9	10
BPD5	199,920	16:19	180	256	120	0.21	4.9	5

*Extension of scan time for later subjects was to enable retrospective motion tracking and correction in quiet-breathing infants.

Table 3

Radiologist Scoring by Category

	Image Quality (1-non-diagnostic, 5-excellent)	Lung Pathology (1-none, 5 severe)	Cardiac Motion (1-none/ insignificant, 5-severe)	Bulk Motion* (1-none/ insignificant, 5-severe)
Radiologist 1	3.75 ± 1.12	3.05 ± 1.28	1.15 ± 0.37	1.85 ± 1.35
Radiologist 2	3.95 ± 0.83	2.95 ± 1.19	1.10 ± 0.31	1.10 ± 0.31

*Difference between bulk motion mean scores from each radiologist was significant ($p < 0.05$)